Flank Wear of Edge-Radiused Cutting Tools under Ideal Straight-Edged Orthogonal Conditions

Raja K. Kountanya[1]
Dept. of Mechanical Engineering
University of Michigan
Ann Arbor, MI 48109-2125

William J. Endres[2]
Dept. of Mechanical Engg. – Engg. Mechanics
Michigan Technological University
Houghton, MI 49931-1295
wjendres@mtu.edu

Abstract

Understanding the effects of tool wear is critical to predicting tool life, the point at which tool performance, in terms of power requirement, dimensional error, surface finish, or chatter, is no longer acceptable. To achieve the long cuts that are required for wear testing while maintaining a clear view of the basic process geometry effects, ideal straight-edged orthogonal conditions are realized in a bar-turning arrangement by employing a specially designed two-tool setup. The data show that increasing edge radius tends to increase wear rate, especially at the initial cut-in wear phase. The data also show that when the uncut chip thickness is less than or equal to the edge radius, forces actually decrease substantially with flank wear until most of the edge radius has been worn away. At that point the forces begin to increase with flank wear in a power-law fashion. This decreasing-then-increasing trend is a result of the parasitic (non chip removing) wear-land force increasing more slowly than the chip-removal force is decreasing. The decrease in chip-removal force with an increase in flank wear results from the blunt edge being effectively sharpened as it is removed by the growing wear land. An empirical model structure is formulated, guided by specific elements of the data, to well represent the force trends with respect to wear and edge radius and to assist in their interpretation. The edge-sharpening concept is further supported by a special experiment in which the edge sharpening effect is studied in the absence of wear land.

[1] Currently with Americas Application Development Center, GE Superabrasives, Worthington, OH, 43085.
[2] Corresponding Author

Nomenclature

F_C Cutting force component (N)
F_T Thrust force component (N)
h Uncut chip thickness (μm)
r_n Edge radius (μm)
l_w Wear-land length (μm)
l_{wc} Critical wear-land length (μm)
w Width of cut (μm)
L_w Non-dimensional wear-land length (–); $L_w = l_w/r_n$
L_{wc} Non-dimensional critical wear-land length (–); $L_{wc} = l_{wc}/r_n$
γ_o Orthogonal rake angle (deg)
α_o Orthogonal clearance angle (deg)
d_w Wear depth (μm)
D_w Non-dimensional wear depth (–); $D_w = d_w/r_n$
F_C' Unit (i.e., per unit width of cut) cutting force (N/mm)
F_T' Unit (i.e., per unit width of cut) thrust force (N/mm)
F_{sf} Force on a fresh sharp tool (N)
F_{bf} Force on a fresh blunt tool (N)
ΔF_{bf} Increase in force, relative to fresh sharp tool, due to a blunt edge (N)
ΔF_{bw} Increase in force, relative to fresh sharp tool, due to a wear-sharpened blunt edge (N)
F_{cr} Chip removal force (N)
F_w Force acting on the wear land (N)
Δ_{ws} Wear sharpening factor — the portion of blunt edge force increase (ΔF_{bf}) present as the edge becomes sharper (–); $\Delta F_{bw} = \Delta_{ws}\Delta F_{bf}$

1 Introduction

Much success has been achieved in accurately predicting machining forces. Moderate success has been achieved in predicting performance measures that stem from those forces, such as form error and stability. However, these successes have been primarily limited to sharp (negligible edge preparation), flat-faced (no chip control), fresh (unworn) tooling. Recent advances have been made, building on earlier efforts [1, 2], to understand and begin to predictively model the effects of edge preparation [3-6] and chip control [7]. These works have taken the natural first step — studies confined to fresh tools. Accounting for edge preparation and chip control is indeed critical to understanding and predicting the performance of the tooling used in practical settings. However, industry practice also motivates an expansion beyond past successes to model

the evolution of cutting tool performance beyond the fresh-tool state. Predicting the change in cutting-tool performance as it wears would ultimately allow one to predict tool life — the point at which the cutting tool's performance is no longer satisfactory and a new tool is needed. The recent "Assessment of Machining Models" effort [8] adopts this mindset as well by setting as its goal the prediction of tool wear as the ultimate assessment measure.

Though chip control geometry may play a role in the growth of flank wear, its primary effect on tool wear is more likely related to crater wear. On the other hand, while edge preparation probably plays a role in the growth of crater wear, intuition, anecdotal evidence and limited published data [9] support the notion that edge preparation is closely linked to flank wear growth. Subsequently, though it is very intuitive that crater wear affects the chip formation process and chip-removal forces [10], other studies note that flank wear does not seem to affect the chip formation process and the resulting chip-removal forces [11].

A rich pool of knowledge has developed on the topic of flank wear for sharp tools. Numerous reports show that forces tend to increase linearly with flank wear, at least up to some level [12-16]. To independently study both flank and crater wear, Stern and Pellini [17] selectively ground a coated tool to selectively expose the substrate. In contrast to the multitude of studies on sharp tools, few works [9] have focused on edge radius effects. For a variety of edge preparations, cutting conditions and cutting tool materials, Mayer and Stauffer [9] measured machining force components in the fresh-tool state and again upon reaching a designated level of flank wear while also documenting the time required to achieve that level of wear. They were able to reconcile the results of the edge-radiused and chamfered tools by representing an edge radius with an effective chamfer angle based on the combination of the feed and edge radius, much the same as did Manjunathaiah and Endres [3] in their study of an equivalent negative rake angle. The work presented here aims to extend the body of knowledge contained in the multitude of tool-wear studies for sharp tools by introducing a blunt or radiused cutting edge.

Going beyond the experimental study of wear progression and its effects, some have attempted to model flank wear. Models of flank wear effects on forces typically employ elastic indentation contact mechanics [15, 18] or a less analytical, more empirical approach [19-22]. Elanayar and Shin [18] note the inclusion of edge radius in their elastic contact model, though it is not explicitly discussed. Related to this contact problem is a recent work by Kountanya [23] that provides a solution to the un-bonded elastic contact problem for arbitrary geometry, such as a cutting tool with a wear land and the remaining unworn portion of the edge radius. Understandably, there is some controversy [24, 25] surrounding any effort that is based on elastic contact since material deformation around the edge radius is known via visual observation to be mostly plastic [5, 6, 26], meaning that one would expect the contact along the adjacent wear land to be plastic as well.

Past efforts on modeling flank wear and effects of flank wear provide a foundation for further efforts and motivation to improve this aspect of machining performance prediction. Today's common use of tooling with an edge preparation, such as an edge chamfer or radius, motivates the revisiting of the flank wear problem to incorporate these tooling characteristics. A better understanding of the basic mechanisms present in the tool-work contact problem would well serve efforts to improve related models or develop new ones that account for edge preparation effects. Therefore, presented here is a careful experimental study of flank wear under conditions of simple process geometry (ideal straight-edged orthogonal cutting) with edge-radiused tools. The data show trends that are not present with up-sharp tooling as has been employed in most of the previous studies. The wealth of knowledge on process mechanics for up-sharp and edge-radiused tools provides a basis for formulating functional relationships that represent those mechanics and aid in interpreting the data.

2 Experimental Study

2.1 Motivation for Ideal Straight-Edged Cutting

Commercial tool wear testing is traditionally conducted using real cutting edge profiles (standard inserts) in their intended application. The usual process of choice is OD bar turning with corner-radiused inserts where large bars can be conveniently used to facilitate the long-duration cuts required in wear testing. In fact, wear testing via OD bar turning is the process upon which the ISO tool-wear testing standard [27] is founded. The standard recommends that tests be conducted at a depth of cut that is at least twice the corner radius in order to minimize the influence of the corner radius. It is well known that the corner radius introduces variation in approach angle as well as a progressive decrease in the uncut chip thickness from the lead edge to the tip of the tool [28, 29], which further motivates using a large depth of cut relative to the corner radius. However, a recent paper by the authors [30] shows that even when the depth of cut is twice the corner radius, the corner radius still has a profound effect on tool (flank) wear. The effect is seen for wear measurements on the lead edge as well as at the tool tip, for both up-sharp tools and edge-radiused tools. Using a 2.5 mm depth of cut, the cited reference presents data for corner radii down to 0.2 mm, at which point the gradient of flank wear versus corner radius is greatest.

The existence of this corner-radius dependency, even when adhering to ISO standards, suggests the following: to isolate the basic flank wear behavior under the conditions for which basic process mechanics models are traditionally formulated (i.e., simple two-dimensional (orthogonal) cutting) one cannot simply rely on using a corner radius that is small or near-zero relative to the depth of cut. The traditional means of achieving ideal/single straight-edged orthogonal cutting is to cut on the end of a thin-walled tube. Unfortunately, this tried-and-true technique is not practical for tool-wear testing since

- each tube specimen permits only a single pass, since the cut consumes the entire wall thickness, and
- a tailstock cannot be used for such an arrangement, which limits the length of a work specimen to about twice the tube diameter.

Therefore, as described below, a two-tool setup has been specially designed and fabricated to provide ideal/single straight-edged orthogonal conditions in a bar-turning arrangement that permits the long-duration cuts required for wear testing.

2.2 Apparatus

Experiments are performed on a manual engine lathe. The setup includes two tools. The first is the *main tool*, the one that performs the single-straight-edged orthogonal cut. This main tool is fixtured in a fashion that is typical for bar turning or tube-end cutting tests — it is mounted to a Kistler 9257B three-component dynamometer that resides on a small tombstone attached to the lathe carriage. The second tool is the *grooving tool* (Kennametal NER 162C with KC710 NG2125LK inserts), which is oriented face down as a component of an additional apparatus that is mounted to the opposite side (rear) of the lathe carriage.

A top-view schematic of the entire assembly is shown in Fig. 1a; a corresponding photograph is shown in Fig. 1b. The grooving tool is used to cut a notch in the end of the bar leaving a small lip at the bar's outer diameter, which is simultaneously removed by the main cutting tool under the single-straight-edged orthogonal conditions sought. The tip of the grooving tool leads the main tool edge (by 1.5 mm here) so that the lip is safely deeper than the greatest feed per revolution. Using a small cross-slide that is integrated into the grooving tool apparatus (see Fig. 1a), the grooving tool is positioned radially (initially and between tool passes) so that the lip's radial (wall) thickness is equivalent to the desired width of cut. The main tool is adjusted radially between tool passes using the lathe's standard cross-slide.

The main tool holder and inserts are ground at their end to remove the corner radius portion so that it does not extend beyond the groove and contact the remaining central portion of the bar-stock. This also allows the edge radius to be very easily measured by viewing the ground-surface (edge cross-section) under a standard high-magnification optical microscope. A sample cross-section is shown in Fig. 2. Furthermore, it is known that the honed edge radius varies sig-

nificantly along the edge in a parabolic fashion with the least variation/gradient occurring at the center of the lead edge [31]. Therefore, more material is ground off than needed to just remove the corner radius so that cutting occurs in this region of smallest variation in edge radius. Removing substantially more than just the corner radius also provides a greater length of rake face so that the chip will lose contact naturally via chip curl, rather than (possibly) prematurely in a reduced-contact fashion.

The final component of the apparatus provides for flank wear measurement without removing the insert or tool holder. This is motivated by past efforts, such as those of Liu and Barash [32, 33] which noted that tool removal and replacement for measurement will cause the tool to wear in a discontinuous fashion, such as to create facets on the tool. Mohun alludes to this point in his comments appended to a paper by McAdams and Rosenthal [12]. Flank wear measurements are made here using a borescope with a right-angle adaptor as shown in Fig. 1c. Figure 1a shows a clearance hole through the tool-mount adaptor and mounting of the borescope to a fine positioning stage. This allows the right-angle adaptor opening to be positioned close to the flank-wear land to in turn provide good magnification. Images are recorded on a computer via a camera and frame capture card. After accounting for all resolutions and magnifications, wear-land measurements can be resolved with confidence in 10 μm increments.

2.3 Test Conditions and Procedure

The same plain carbon steel work material used in the authors' earlier work on corner-radius effects [30] was employed for the tests of the current study. Experience with this work material had indicated the absence of a built-up edge for cutting speeds of 600 sfpm and above. More details may be found in the cited reference. All cuts are conducted dry at a 3.18 mm width of cut, w. Since the focus is on effects of edge radius, uncut chip thickness h and cutting speed are held constant at 37 μm (0.0015 in.) and 366 m/min (1200 fpm), respectively. The uncut chip thickness is chosen so that its ratio to edge radius, r_n, varies from below unity to well above unity

Table 1 Edge radius (μm) replication groupings

Edge Radius Group	Actual Edge Radii	Edge Radius Group	Actual Edge Radii
Up-sharp	8	100	97
	9		99
	10	110	108
	12		113
27	27	125	126
36	36		126
60	60		128
83	83		

across the range of edge radius, the maximum considered being 125 μm and the minimum being approximately 10 μm for the up-sharp tools. Clearly, the ratio of the width of cut to the uncut chip thickness, as well as to edge radius ($w/r_n > 25$), is sufficiently large to maintain predominantly plane-strain conditions in chip formation and minimal side flow under the edge. The main tool is a CTGPR-164C (zero lead, +5° side rake) that is modified by grinding the end as noted above (corner-radius removal) and milling the shank to realize a zero rake angle. Preliminary tests comparing K313 (uncoated C3-C4) and K420 (uncoated C6) grade inserts showed the K313 grade to exhibit large levels of crater wear relative to flank wear, whereas the K420 grade showed only minimal cratering. Therefore, an uncoated C6 grade was chosen for the final experiment. The TPG 432 inserts used provide an 11-degree clearance angle. Target edge radius levels are up-sharp (~5 μm), 25, 50, 100 and 150 μm. The experiment is designed to have three replications of each of the five target edge radius levels. However, due to the poor consistency that is common in honed edge radii, the actual edge radius values vary in many cases from the target levels. Therefore, only some of the fifteen tests/tools can be grouped to provide a sense of replication (see Table 1).

The bar-stock is 600 mm in length and ranges from 125 mm in diameter initially down to 50 mm, at which point it is discarded to avoid an excessive increase in its overall temperature. Each

test is interrupted at durations of 15, 30, 45, 60, 75, 105, 135, 180, 240, 300, 360, 420, 480, … and 900 seconds to measure flank wear. Interruptions are scheduled more frequently early in the cut to capture the rapid-wear cut-in phase [34]. Force data represent the average force computed over the final 25% of the preceding cutting interval just prior to the interruption for the respective wear measurement. The forces of interest are the thrust force F_T (equivalent to the feed force) and the cutting force F_C (equivalent to the tangential force). Resetting the charge amplifier at each measurement interruption alleviates any potential drift problems.

2.4 Data

The wear evolution data are shown in Fig. 3 where third-order polynomial curve fits have been added to help one's eye track each series. Some of the jaggedness in the data is a result of the wear measurement resolution being 10 μm. Though the focus of this work is not on wear rate/evolution in particular, it is fair to comment on the evolution data in that there is substantial inconsistency within each grouping of multiple edge radii (see Table 1) as well as the ordering of wear rate across some of the edge radius levels in general. For instance, in the top plot, while the 8-, 9- and 10-μm tools track each other fairly well, the 8-μm tool exhibits the highest wear of those three. Not only would intuition dictate that higher wear occur for larger edge radii, the findings of Mayer and Stauffer [9] and Endres and Kountanya [30] solidly support that trend. This mis-ordering is likely a product of experimental error. The 12-μm tool has noticeably higher wear, but since that edge radius is 25-50% larger than the others, that difference is not unreasonable. However, while the middle plot shows the 97- and 99-μm tools to track consistently, there is again substantial mis-ordering of wear level with edge radius level across all the tools shown in that plot. Finally, in the bottom plot, the 108- and 113-μm tools differ enormously as does the 128-μm tool relative to the 126-μm tool.

The repeatability of the data presented by Endres and Kountanya [30], where each test is replicated three times, is far superior. We speculate that the single main difference in the two test plans is the likely cause. That is, in the work of Endres and Kountanya [30], the three

plans is the likely cause. That is, in the work of Endres and Kountanya [30], the three replications are conducted on three corners of the same (triangular) insert. Here, the replications are conducted on different inserts, due to the need to grind the corner. The likely explanation is therefore tool material variation. This has not been further pursued via micrographs or microhardness testing since, as stated, the focus is on the coupled effects of wear and edge radius on forces.

The above inconsistencies aside, there is one wear-versus-time characteristic that seems to be consistent. Figure 4 shows the dependence on edge radius of the 15-second wear measurement, considered to be representative of the cut-in wear. There is clearly some "noise", but for the most part there is a fairly strong linear ($R^2 = 0.8$) or exponential ($R^2 = 0.9$) increase in cut-in wear with increasing edge radius. Most of the deviation from the trend-lines occurs at the large edge radii. Due to the low h/r_n values for these tools, which result in highly inefficient cuts, the larger edge-radiused tools would tend to run substantially hotter than the sharper tools. Noting that much of the aforementioned wear-evolution variation occurs at higher wear levels, a condition that also increases tool temperature, it appears that higher temperature is correlated to the inconsistencies in wear versus edge radius. We hypothesize the following:

- the base hardness may be comparable across all the tools while the hardness decay rate with temperature due to softening may vary across the tools;
- subsequently, the higher temperature conditions (larger edge radius and/or high wear) increase sensitivity to this supposed variation in the tool material hot-hardness decay.

The unit force (force per unit width of cut) data are plotted versus flank-wear land length in Fig. 5 where quadratic curve fits have been added. Here, the potential insert-to-insert variation is not an issue since the relationship is the measured force versus the measured tool geometry, each of which should be relatively independent of tool-material properties. The only potential plague to these data is the 10-μm resolution in the wear data. Here, we see something quite interesting and initially counterintuitive — forces for the tools of larger edge radius, in particular the thrust force but also the cutting force, initially decrease as wear increases. This finding is the topic of the ensuing data analysis and discussion.

3 Data Analysis and Discussion

3.1 Decreasing Force with Wear

From the data in Fig. 5, the general tendency is a monotonic increase in force with wear for lower edge radii where $h/r_n > 1$ and a decreasing-then-increasing trend for more blunt tools where $h/r_n < 1$. For the sake of convenience in the discussion, tools with $h/r_n \geq 1$ will be referred to as "sharp" whereas those with $h/r_n < 1$ will be referred to as "blunt". Though not shown for the sake of brevity, the same trend exists for the resultant force orientation relative to the cutting direction, which contradicts methods used in wear monitoring [35] where the force ratio (F_T/F_C) is assumed to increase monotonically with wear.

The sharp tools exhibit the trend that is seen in numerous past studies and is generally agreed upon — a monotonic increase in force with flank wear [36]. The initial decrease in force with increasing wear for the blunt tools is in disagreement. We explain this decrease to be the result of the initial progression of the wear land sharpening the blunt edge by gradually removing the edge radius. The improved efficiency and reduced chip-removal force that come with a sharper edge outbalance the increased parasitic wear-land force that grows with the wear land. At some level of wear the edge radius is *effectively* removed, meaning that with further increases in wear-land length the decay in the chip-removal force is outweighed by the growth in the wear-land force. Beyond this wear level the total force (chip removal plus wear land) must then increase.

In support of this conjecture, additional tests are conducted while sectioning and photographing the edge profile at various stages of the cut. Before each photograph is taken, the edge is re-sectioned leaving some of the original width of cut mark on the edge for continued testing; subsequent cutting occurs partially on the original width of cut mark and partially on a fresh potion of the edge. About three sections can be made before the entire original width of cut mark is removed. Figure 6 shows the evolution of the flank wear process where the edge bluntness (r_n = 125 μm) of the fresh tool in image 1 is gradually removed by the wear land. In some images (2 and 3) the edge bluntness deviates from the basic radiused shape of the original edge; the edge

then regains the radiused shape in image 4 (note that each image results from re-sectioning the tool further down the edge, which explains how the edge seems to regain its radiused shape, as the chip contact pressure can vary across the width (into page) of contact). Deviation from the basic radiused shape is consistent with the apparent negative rake effect on chip flow that is known to occur when h/r_n is much smaller than unity (equal to 38/125 = 0.3 here) [3]. Despite some deviations from the basic radiused shape, general edge "bluntness" is present and to a decreasing degree as the tool wears. Figure 7 shows the case for a smaller edge radius (r_n = 70 μm) for which h/r_n = 1.0 where the edge radius remains fairly in tact until an enormous level of flank wear at which point significant cratering has occurred as well.

The geometry of a flank wear land imposed on an edge-radiused tool is shown in Fig. 8, where l_w is the wear-land length, d_w is the wear depth, γ_o is the rake angle, α_o is the clearance angle, R is the resultant machining force, and l_{wc} is the critical wear-land length at which the entire edge radius is worn away. The expression relating wear depth and wear-land length is best enumerated computationally in non-dimensional terms ($D_w = d_w/r_n$ and $L_w = l_w/r_n$), results of which are shown in Fig. 9 for the zero-rake, 11-degree clearance tool used in the tests. The edge radius is fully removed when $D_w = 1 + \sin\gamma_o$, or $D_w = 1$ here, which corresponds to a critical non-dimensional wear-land length $L_{wc} = l_{wc}/r_n$ of about six.

The blunt-tool force data are plotted versus non-dimensional wear-land length (L_w) in Fig. 10, which shows most of the curves to reach a minimum around L_w = 4 or 5. Referring to Fig. 9 shows L_w = 4.5 to correspond to $D_w \approx 0.67$, which corresponds to only the upper 18 degrees ($\tan^{-1}(1-0.67)$) of the edge radius still being present. This is reasonable since, as described above, the total force should begin to increase not when the decay in chip-removal force becomes zero (complete removal of the edge radius when $L_w = L_{wc}$), but rather when the rate of wear-land force increase exceeds the rate of chip-removal force decrease. The latter must occur at some point slightly before the edge radius is completely removed at which point the chip-removal force is still gradually decreasing. In fact, it is known that as h/r_n increases the effect of

edge radius on chip removal is diminished. Therefore, for larger h/r_n (smaller r_n here for the constant h considered) it is likely that the minimum point would occur when an even greater percentage of the edge radius is still present (lower L_w) since the edge radius has less effect on chip removal in the first place when h/r_n is larger. So, it may be the case that the particular location of the minimum point is relatively constant for a given h/r_n, not for a given h as is the case in this experiment. That issue is not explored here; it is a good topic of continuing study.

The edge-sharpening explanation offered here, in conjunction with the quantitative assessment and observation of when the edge radius is effectively removed ($L_w \approx$ 4-5), explains why this decreasing-then-increasing trend went unnoticed in the two previous works that studied flank wear with blunt tools [9, 18]. In the data published by Mayer and Stauffer [9] a consistent decrease in force from the start to the end of cut is seen for the more blunt tools in their low-speed tests; it just is not noted and discussed in the text. Their high-speed tests, on the other hand, show an increase in forces from the start to the end of the cut. The reason for this may be explained in terms of the level of wear at the end of the cut relative to the edge radius. For the high-speed tests, the end-of-cut wear-land lengths are quite large relative to the edge radius, meaning that the forces measured at the end of the cut are well past their minimum point (at $L_w \approx$ 4-5). For the low-speed blunt-tool tests, the non-dimensional wear level has not reached this point by the end of the cut, so the forces measured are still decreasing, and hence are lower at the end of the cut compared to the start of the cut. In the work of Elanayar and Shin [18], the cut-in wear (or lowest reported wear levels) is around 50 μm. Since edge radii measurements are not reported, it is difficult to judge whether there might have been any decrease in forces early on when L_w was below 4. If their tools were up-sharp, implying an edge radius below 10 μm, the first measurements of 50 μm would in fact be beyond the minimum-force point (L_w = 5) and the presented data, which show a monotonic increase in force with wear-land length, would be expected.

3.2 Coupled Effect of Flank Wear and Edge Radius

The unit force data are further explored to see if there exists a representation in which the effect of edge radius is removed — in other words, one where all the data fall together into a single trend. The intent is not to propose some predictive approach, but rather to physically rationalize the effects of edge radius and wear land as rooted in process mechanics.

Viewing the unit force versus the non-dimensional wear-land length does not unify the data as evidenced by the notably different curves in Fig. 10 as opposed to a convergence to a set of nearly identical curves. However, non-dimensional wear-land length does unify the results when the other variable is the unit force (F_C' or F_T', the prime indicating "unit" force) divided by the non-dimensional wear-land length, as shown in Fig. 11. The result of this representation is the function form

$$\frac{F_\bullet'}{L_w} = c_0 + c_1 \, \mathrm{e}^{-L_w} + \frac{c_2}{L_w}, \quad \bullet = C, T, \tag{1}$$

which produces R^2 values of about 0.9 compared to 0.09 when fitting unit force directly against non-dimensional wear-land length, as in Fig. 10 but for all tools/data.

The coefficients of Eq. (1) (c_0, c_1, c_2) are (–0.587, –33.2, 145) for the cutting direction and (1.21, 126, 105) for the thrust direction. The changes in the signs of the coefficients for the two directions are an undesirable inconsistency. Furthermore, the model fitting cannot accommodate the fresh-tool ($L_w = 0$) forces. These model failures are likely the result of Eq. (1) not being born of any physical reasoning. Noting that the dependent variable of Eq. (1) is force per unit wear-land area, one must ask if there should be any consistent relation since the total force is clearly made up of both the chip-removal and wear-contact mechanisms, not just that arising from the wear contact alone.

Better success is achieved by approaching the problem from the opposite direction — building a function form based on knowledge of trends in the process mechanics rather than finding a function form that works and then trying to explain it based on mechanics.

3.2.1 A Mechanics-Driven Model

The first element of the unit force (cutting or thrust) is its value for a tool of zero edge radius and no (flank) wear, i.e., a fresh, sharp tool. This can be thought of as the baseline — a constant with respect to edge radius and wear-land length — and is referred to as F_{sf}, the *fresh-sharp force*. When an edge radius is introduced, for a given constant uncut chip thickness, fresh-tool forces should increase as edge radius increases. The "fresh-state" forces are extracted from the first two seconds of each wear test discussed thus far. Force-versus-time data support the assumption made here — that minimal wear accumulates in the first two seconds — even for the very blunt tools where the 15-second cut-in wear is quite large.

Figure 12a shows how the unit force changes with edge radius for all tools considered. The force plotted is F_{bf}, the *fresh-blunt force*, which is made up of a constant term, F_{sf}, and a proportional term such that

$$F_{bf} = F_{sf} + \Delta F_{bf}, \quad \Delta F_{bf} = c_b r_n, \tag{2}$$

where ΔF_{bf} is the *fresh-blunt force rise*. Coefficients of this fit are shown in the figure. A power-law form for ΔF_{bf} (i.e., $\Delta F_{bf} = c_{b1} r_n^{c_{b2}}$) yields exponents ($c_{b2}$) that differ from unity in a manner that is not significant. This may not be the case for all work materials; a power-law form may be a more appropriate form to consider in general.

The wear land then affects the total force in two ways: by affecting the chip-removal force and also by introducing a parasitic wear-land force. The chip-removal force thus far studied ($F_{bf} = F_{sf} + \Delta F_{bf}$) is affected by the blunt edge being sharpened as the wear-land length increases, as depicted in Fig. 8. This causes ΔF_{bw}, the *worn-blunt force rise*, to decrease from its fresh-tool value of ΔF_{bf}. The decrease in ΔF_{bw} with wear-land length should occur at a decreasing rate and such that ΔF_{bw} becomes zero when the edge bluntness is fully removed by the wear land, at which point the total chip-removal force becomes F_{sf}. This is achieved by scaling ΔF_{bf} by Δ_{ws}, the *wear-sharpening factor* — a decaying (negative-exponent) exponential. The result is a net chip removal force of

$$F_{cr} = F_{sf} + \Delta F_{bw}, \quad \Delta F_{bw} = \Delta F_{bf}\,\Delta_{ws}, \tag{3}$$

where ΔF_{bf} is given in Eq. (2). Since a decaying exponential never reaches zero, it is considered here to be effectively zero when it reaches approximately 0.05, which occurs when its exponent is about –3. The edge radius is completely removed when L_w reaches its critical value L_{wc}. Therefore, the proposed exponent is $-3L_w/L_{wc}$. For the 11-degree clearance tools here, $L_{wc} \approx 6$ (see Fig. 9), so the proposed exponent for these data is $-0.5L_w$.

The second effect of the wear land is the addition of its parasitic *wear-land force*, F_w. Only those data for which $L_w > L_{wc}$ are considered so that the wear-land force can be computed by subtracting F_{sf} from the total force measurements. In other words, no remnants of edge radius are present when $L_w > L_{wc}$, so the wear-land force is simply all the force in excess of the fresh-sharp force F_{sf}. Figure 12b shows the unit wear-land force plotted against wear-land length. Past studies [12-16] and elastic contact mechanics suggest that this force should behave linearly with wear-land length. However, the linear fits shown in the figure, forced to have a zero intercept for obvious physical reasons ($F_w = 0$ for zero wear, by definition), provide R^2 values of 0.25 and 0.31. Clearly, the data are better represented with the power-law fits shown. Therefore, the wear-land force is modeled to behave as

$$F_w = c_{w1} l_w^{\,c_{w2}}, \tag{4}$$

which encompasses cases where the behavior is linear by c_{w2} becoming unity.

Given the above, the complete force function is

$$\begin{aligned} F &= F_{sf} + \Delta F_{bw} + F_w \\ &= F_{sf} + c_b r_n \mathrm{e}^{-0.5L_w} + c_{w1} l_w^{\,c_{w2}}, \end{aligned} \tag{5}$$

where the constants F_{sf}, c_b, c_{w1}, and c_{w2} are obtained from specific portions of the data (see Fig. 12) and r_n and l_w are in μm and the unit force is in N/mm. As an alternative, nonlinear regression can be applied to fit this function form to all the wear data. This yields

Table 2 RMS percent error for the two empirical models

Direction	All-at-Once	Piece-by-Piece
Cutting	6.83	9.62
Thrust	12.5	19.1

$$F_C' = 101 + 0.262 r_n \, e^{-0.5 L_w} + 1.99 l_w^{\,0.521}$$
$$\text{and} \qquad (6)$$
$$F_T' = 80.9 + 1.10 r_n \, e^{-0.5 L_w} + 1.38 l_w^{\,0.555}.$$

This "all-at-once" regression fit is shown graphically in Fig. 13 (thrust direction) to well characterize the physical data. The "piece-by-piece" result (using coefficients from Fig. 12) compares quite favorably with the all-at-once regression result. Figure 14 shows the percent deviation of the piece-by-piece model relative to the "best-fit" all-at-once model. The deviation range is smaller for the cutting direction and, for both directions, is smallest (including most negative) and relatively constant for $L_w > L_{wc}$. The RMS percent error of the two empirical models, relative to the actual data, is shown in Table 2. The piece-by-piece model exhibits slightly more error, which is to be expected since the all-at-once model is truly a best "fit" to all the data as compared to the piece-by-piece model being a best "match" to the mechanics and a best "fit" only to each respective subset of data. Since the piece-by-piece model is based purely on specific elements of the data set that have explicit links to the physics of the edge and wear-land effects, the closeness of the two in terms of the end result is very encouraging. The individual effects of edge radius and wear land are probably better represented by the piece-by-piece model since it does not spread the effects of wear land across all the force elements in order to get a mathematical best fit, which is what happens in fitting the all-at-once model, where the fitting error is distributed arbitrarily among the constants of the function form.

3.2.2 Edge-Sharpening Experiment

The effects of the edge radius alone (i.e., in its fresh state), and the wear-land alone (i.e., after complete edge radius removal), are supported above by extracting specific force data from the

full set of wear-test data. However, no manner of extracting data from the wear tests can offer support for the proposed wear-sharpening factor Δ_{ws}, though it seems to work well in the regression results of Eq. (6). Tests to confirm the proposed wear-sharpening factor are devised as follows. The blunt edge is incrementally sharpened by removing layers from the flank face with a grinding wheel, as shown in Fig. 15. Short cutting tests are conducted between flank-grinding increments to mimic the gradual (incremental) removal of the edge radius by the wear land. This approach changes the edge geometry in the same way as wear-land growth does, while allowing forces to be collected without the parasitic wear-land force being present.

Tests are conducted for three "replications" at edge radii of 107, 120 and 120 μm. Of interest is how $\Delta_{ws} = \Delta F_{bw}/\Delta F_{bf}$ (per Eq. (3)), changes with non-dimensional wear-land length L_w. The force measured at the end of each test, when the entire edge radius has been completely ground away, is that of the fresh-sharp tool. Averaging this final measurement across the three tests (edge radii) provides the value for F_{sf}. The worn-blunt force rise, ΔF_{bw}, is obtained for each measurement by subtracting F_{sf} from that measurement (equivalent to F_{cr} in Eq. (3)). The fresh-blunt force F_{bf} for a given edge radius is the first force measurement, for that edge radius, taken when the entire edge radius is present. The fresh-blunt force rise, ΔF_{bf}, is F_{bf} less F_{sf}. Based on Eq. (3) and the discussion here, the wear-sharpening factor for measurement j of edge radius i is

$$\Delta_{ws_{ij}} = \frac{\Delta F_{bw_{ij}}}{\Delta F_{bf_i}} = \frac{F_{cr_{ij}} - F_{sf}}{F_{bf_i} - F_{sf}} \, .$$

The computed wear-sharpening factor is plotted against equivalent non-dimensional wear-land length L_w in Fig. 16. The data from all three replications (edge radii), for both the cutting and thrust directions, fall into a single trend. Also graphed are the proposed wear-sharpening factor form of $\Delta_{ws} = \mathrm{e}^{-0.5L_w}$ and two regression-fit exponentials. The first (Fit 1) has an intercept of unity imposed since, by definition, $\Delta_{ws} = 1$ when $L_w = 0$. The proposed form matches this regression result, and hence the data, quite well despite the regression exponent of $-0.524L_w$ being slightly different than the proposed $-0.5L_w$. The second regression-fit exponential (Fit 2) does

not have a unity intercept imposed. In this case, the exponent matches that proposed ($-0.5L_w$) but the magnitude (intercept) is off by 9%.

Despite the minor differences between the proposed coefficients compared to those of the regression fits, the experiment confirms the edge-sharpening effect of the wear land. It also quantitatively supports the proposed exponentially decaying wear-sharpening factor, in particular its $-3L_w/L_{wc}$ exponent that comes forth from the basic geometry of the edge-sharpening problem. In effect, all pieces of the piece-by-piece model have been verified experimentally.

4 Conclusions

Reported here is a new experimental approach that permits the study of tool wear under ideal single-straight-edged conditions while measuring flank wear without disturbing the tool. Tool wear evolution was observed and machining force components were measured for cutting with edge-radiused tools at a fixed uncut chip thickness, cutting speed and rake angle using uncoated carbide (WC) tools. Applying knowledge of process mechanics and specific data extractions, an empirical function form for the process force was formulated to rationalize the simultaneous effects of edge radius and wear-land length. That empirical function along with the nature of the experiment itself provides an unclouded assessment of the basic interactions of edge radius and wear-land, which leads to the following conclusions:

- Cut-in wear increases exponentially with edge radius and is quite large for more blunt tools, at least at the cutting speed considered here.
- The measured forces increase monotonically with an increase in wear-land length for sharp tools, i.e., those for which the ratio of uncut chip thickness (h) to edge radius (r_n) is greater than unity.
- For blunt tools ($h/r_n < 1$), the measured forces initially decrease with an increase in wear-land length, and then begin to increase once the wear-land length exceeds about 4-5 times the edge radius (for the 11-degree clearance angle considered).
- The decreasing-then-increasing trend exists for the cutting component, more so as the tool gets more blunt. This trend is far more noticeable for the thrust force component, as would be expected based on past findings that both edge radius and flank wear more strongly affect the thrust force.
- The decreasing-then-increasing trend results from the blunt edge being sharpened (gradual removal of the edge radius) as the wear-land grows. This phenomenon as well as the edge-sharpening rate is confirmed though a separate complementary edge-sharpening experiment.

- The parasitic wear-land force increases with wear-land length in a fashion better represented as a power law with its exponent less than unity than a linear form usually considered.

Acknowledgements

The authors wish to acknowledge the support of this research by the National Science Foundation through CAREER grant DMI-9734147. Sincere thanks are in order for Mr. Ray Moring of Kennametal, Inc. for providing tooling and Mr. Bill Shaffer of Conicity Technologies for providing edge-honing services. The assistance of doctoral candidate Ms. Zhen Zhang in supplemental testing to acquire the wear evolution images is greatly appreciated.

References

[1] Albrecht, P., 1960, "New Developments in the Theory of the Metal Cutting Process Part-I. The Ploughing Process in Metal Cutting," ASME J. Eng. Ind., **82**, 348-358.

[2] Nakayama, K., and Tamura, K., 1968, "Size Effect in Metal Cutting Force," ASME J. Eng. Ind., **90**, pp. 119-126.

[3] Manjunathaiah, J., and Endres, W. J., 2000, "A Study of Apparent Negative Rake Angle and its Effects on Shear Angle during Orthogonal Cutting with Edge-Radiused Tools," *Trans. NAMRI/SME*, **28**, 197-202.

[4] Manjunathaiah, J., and Endres, W. J., 2000, "A New Model and Analysis of Orthogonal Machining with an Edge-Radiused Tool," ASME J. Mfg. Sci. Engg., **122**, 384-390.

[5] Schimmel, R. J., Endres, W. J., and Stevenson, R., 2002, "Application of an Internally Consistent Material Model to Determine the Effect of Tool Edge Geometry in Orthogonal Machining," to appear Aug., ASME J. Man. Sci. Eng., **124**, 536-543.

[6] Kountanya, R., and Endres, W. J., 2001, "A High-Magnification Experimental Study of Orthogonal Cutting with Edge-Honed Tools," *Proc. ASME IMECE*, New York, CDROM, **3**.

[7] Jawahir, I. S., and van Luttervelt, C. A., 1993, "Recent Developments in Chip Control Research and Applications," *CIRP Annals*, **42**, 659-693.

[8] Ivester, R. W., Kennedy, M., Davies, M., Stevenson, R., Thiele, J., Furness, R., and Athavale, S., 2000, "Assessment of Machining Models: Progress Report," *Mach. Sci. and Tech.*, **4**, 511-538.

[9] Mayer, J. E., and Stauffer, D. J., 1973, "Effects of Tool Edge Hone and Chamfer on Wear Life," *SME Technical Paper*, **MR73-907**, 20.

[10] Friedman, M. Y., and Lenz, E., 1973, "Effect of Thermal Conductivity of Tool Material on Cutting Forces and Crater Wear Rate," Wear, **25**, 39-44.

[11] Oraby, S. E., and Hayhurst, D. R., 1991, "Development of Models for Tool Wear Force Relationships in Metal Cutting," Int. J. Mech. Sci., **33**, pp. 125-138.

[12] McAdams, H. T., and Rosenthal, P., 1961, "Forces on a Worn Cutting Tool," ASME J. Eng. Ind., **83**, pp. 505-512.

[13] Taraman, K., Swando, R., and Yamaguchi, W., 1974, "Relationships between Tool Forces and Flank Wear," *SME Tech Paper*, **MR74**, 11-15.

[14] Wang, J. Y., and Liu, C. R., 1998, "New Concept for Decoupling the Cutting Forces due to Tool Flank Wear and Chip Formation in Hard Turning," J. Mach. Sci. and Tech.,

2, 77-90.
[15] Smithey, D. W., Kapoor, S. G., and DeVor, R. E., 2000, "Worn Tool Force Model for Three-Dimensional cutting Operations," Int. J. Mach. Tools Man., **40**, 1929-1950.
[16] Smithey, D. W., Kapoor, S. G., and DeVor, R. E., 2001, "A New Mechanistic Model for Predicting Worn Tool Cutting Forces," J. Mach. Sci. and Tech., **5**, 23-42.
[17] Stern, E. L., and Pellini, R. P., 1993, "Study on the Effect of Tool Wear on Machining Forces," *Manuf. Sci. and Eng.*, **ASME-PED 64**, 445-451.
[18] Elanayar, S., and Shin, Y. C., 1996, "Modeling of Tool Forces for Worn Tools: Flank Wear Effects," ASME J. Man. Sci. Eng., **118**, 359-366.
[19] Dearnley, P. A., 1985, "Rake and Flank Wear Mechanisms of Coated and Uncoated Cemented Carbides," ASME J. Eng. Mat. Technol., **107**, 68-82.
[20] Fang, X. D., 1994, "Experimental Investigation of Overall Machining Performance with Overall Progressive Tool Wear at Different Tool Faces." Wear, **173**, 171-178.
[21] Kountanya, R., and Kwon, P., 1999, "Experimental Observations on Flank Wear in Machining Spherodized Plain Carbon Steels," Trib. Trans., **42**, 265-272.
[22] Chen, W., 2000, "Cutting Forces and Surface Finish when Machining Medium Hardness Steel using CBN Tools," Int. J. Mach. Tools Man., **40**, 455-466.
[23] Kountanya, R., 2001, "Plane Contact with a Rigid Indenter," J. Mechanika, **5**, 10-15.
[24] Waldorf, D. J., 1996, "Shearing, Ploughing and Wear in Orthogonal Cutting," Ph.D. Thesis, University of Illinois, Urbana.
[25] Manjunathaiah, J., 1998, "Analysis and a New Model for the Orthogonal Machining Process in the Presence of Edge-Radiused (Non-sharp) Tools," Ph.D. Thesis, University of Michigan, Ann Arbor.
[26] Warnecke, G., 1977, "A New Method for Visualizing the Cutting Process," *Man. Eng. Trans.*, 229-236.
[27] ISO, 1993, "Tool Life Testing with Single Point Turning Tools," *ISO 3685:1993(E).*
[28] Young, H. T., Mathew, P., and Oxley, P. L. B., 1987, "Allowing for Nose Radius Effects in Predicting the Chip Flow Direction and Cutting Forces in Bar Turning," *Proc. of the Inst. of Mech. Eng., Part C: Mech. Engg. Sci.*, **201**, 213-226.
[29] Endres, W. J., 1995, "Approximations for Efficient Analytical Computation of Effective Lead Angle in Mechanistic Turning, Boring and Face Milling Models," *Tech. Papers. of NAMRI/SME*, **23**, 147-152.
[30] Endres, W. J., and Kountanya, R., 2002, "The Effects of Corner Radius and Edge Radius on Tool Flank Wear," *Trans. NAMRI/SME*, **30**, 401-407.
[31] Schimmel, R., Manjunathaiah, J., and Endres, W. J., 2000b, "Edge radius variability and force measurement considerations," ASME J. Man. Sci. Eng., **122**, 590-593.
[32] Liu, C. R., and Barash, M. M., 1976a, "Mechanical State of the Sublayer of a Surface Generated by Chip-Removal Process — 1. Cutting with a Sharp Tool," ASME J. Eng. Ind., **98**, 1192-1201.
[33] Liu, C. R., and Barash, M. M., 1976b, "Mechanical State of the Sublayer of a Surface Generated by Chip-Removal Process — 2. Cutting with a Tool with Flank Wear," ASME J. Eng. Ind., **98**, 1202-1208.
[34] Chubb, J. P., and Billingham, J., 1980, "Coated Cutting Tools — A Study of Wear Mechanisms in High Speed Machining," Wear, **61**, 283-293.
[35] Ravindra, H. V., Srinivasa, Y. G., and Krishnamurthy, R., 1993, "Modelling of Tool Wear based on Cutting Forces in Turning," Wear, **169**, pp. 25-32.
[36] Schimmel, R. J., Endres, W. J., and Stevenson, R., 2000a, "Effect of Zero-Clearance Lands in Orthogonal Machining in Light of an Internally Consistent Material Model." *Mach. Sci. and Tech.*, **4**, 101-125.

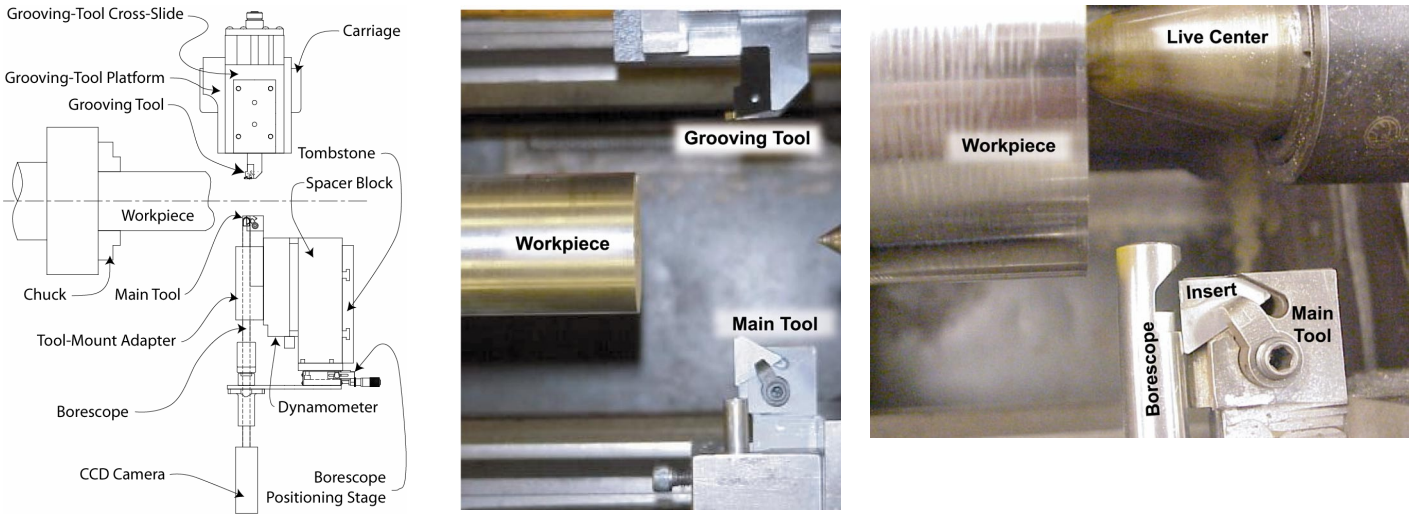

(a) (b) (c)

Figure 1 Experimental apparatus: (a) schematic of entire setup, (b) photo of work zone, (c) photo of main tool and borescope used for flank wear measurement

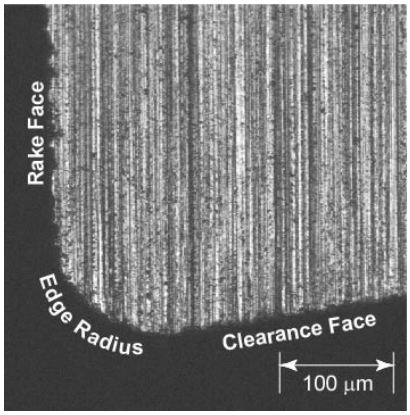

Figure 2 Sample edge cross-section as viewed under optical microscope at 100X

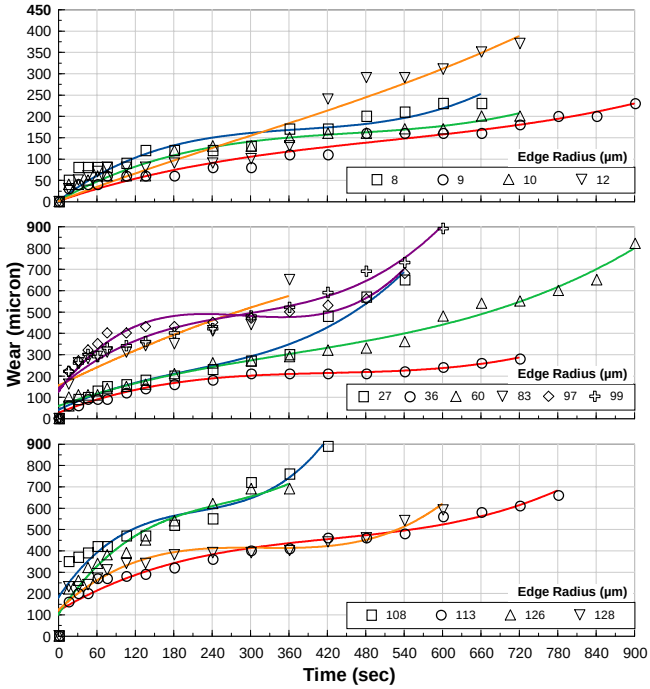

Figure 3 Flank-wear land length evolution: (top) up-sharp, (middle) moderate edge radius, and (bottom) large edge radius

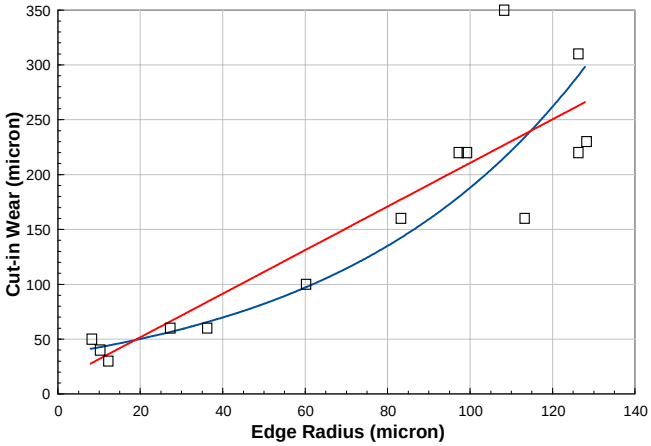

Figure 4 Dependence of cut-in wear on edge radius

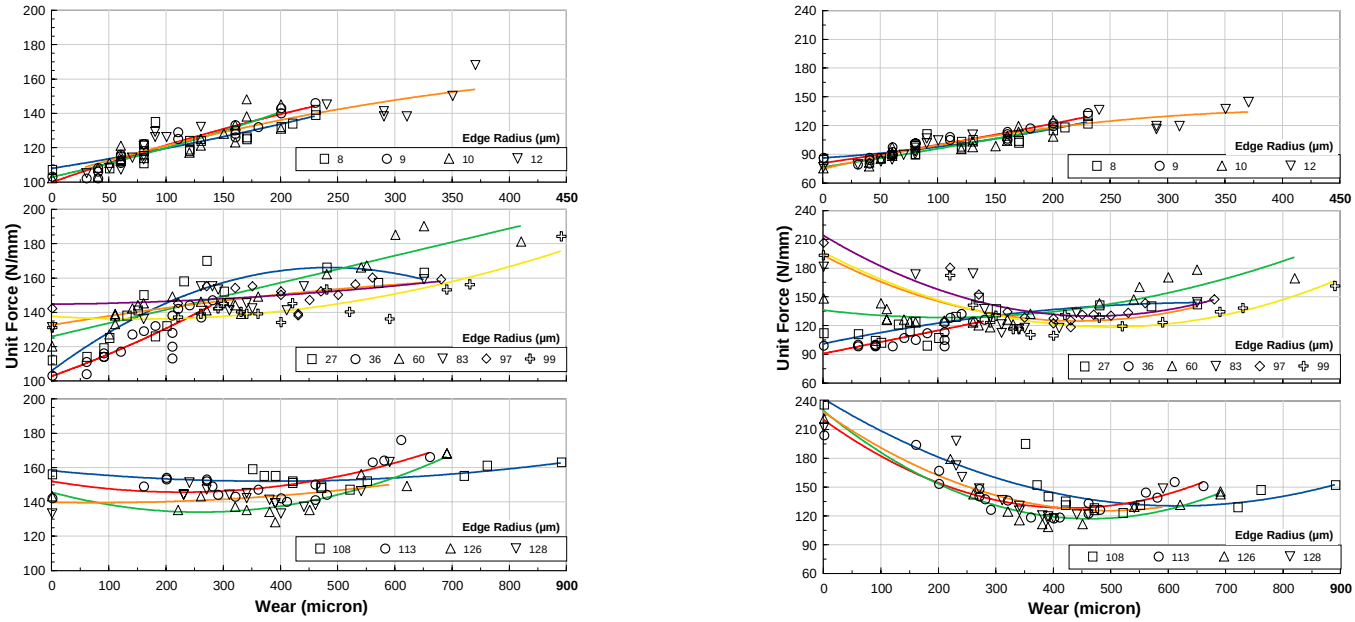

(a) (b)

Figure 5 Unit force versus flank-wear land length: (top) up-sharp, (middle) moderate edge radius, and (bottom) large edge radius: (a) cutting direction, (b) thrust direction

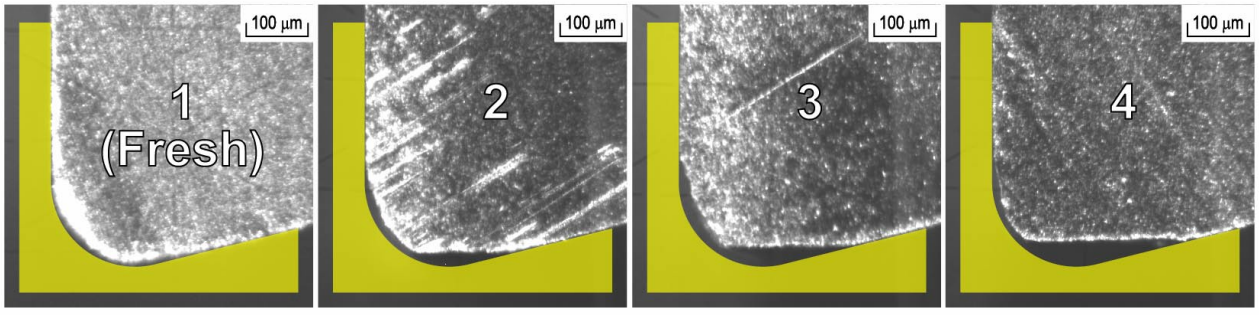

Figure 6 Evolving geometry of a flank-worn, edge-radiused tool (annotation shows relative boundary of the fresh tool); r_n = 125 µm, h = 38 µm

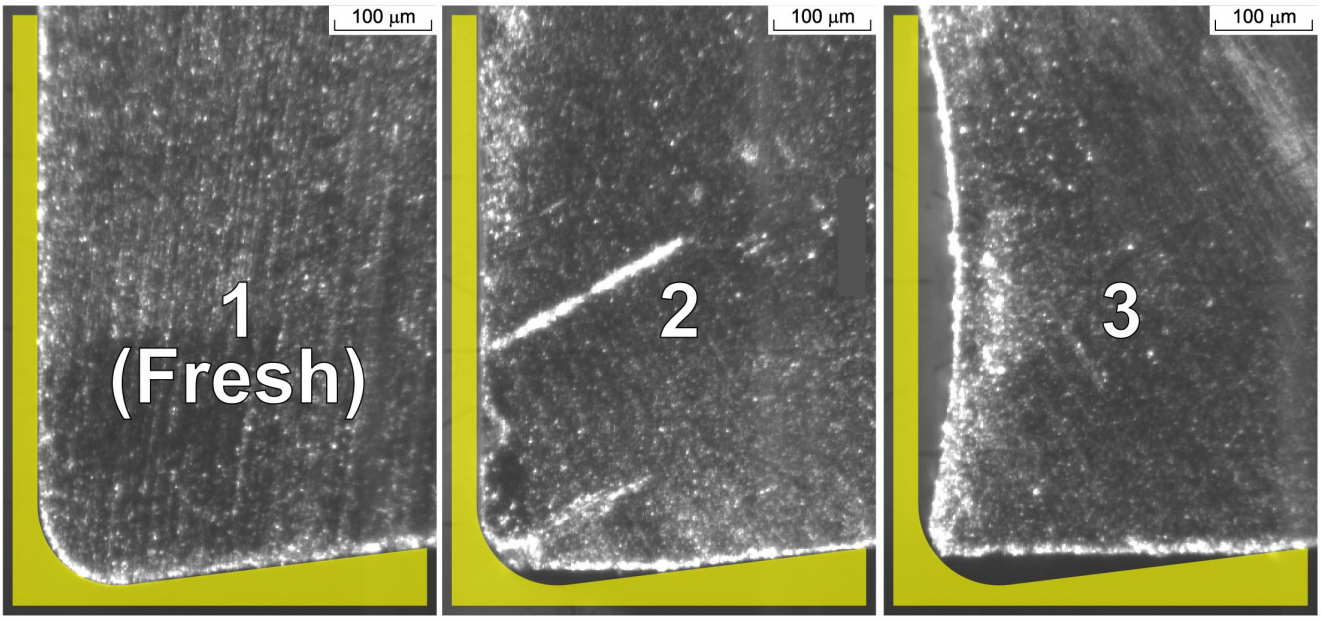

Figure 7 Evolving geometry of a flank-worn, edge-radiused tool (annotation shows relative boundary of the fresh tool); r_n = 70 µm, h = 70 µm

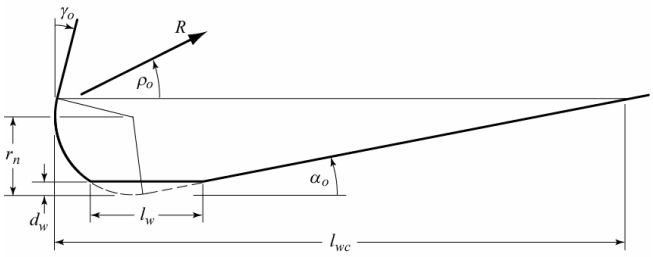

Figure 8 Geometry of an edge-radiused tool with a flank wear land

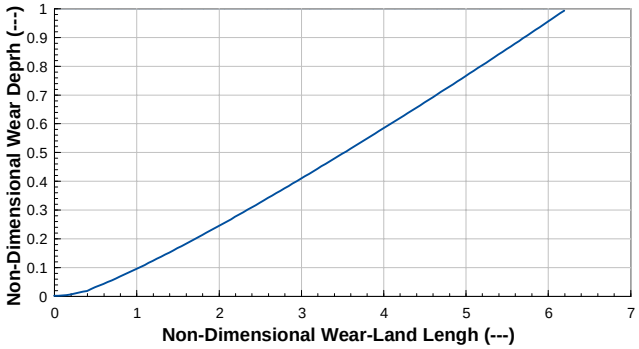

Figure 9 Non-dimensional wear-land depth versus length for zero rake and 11-degree clearance

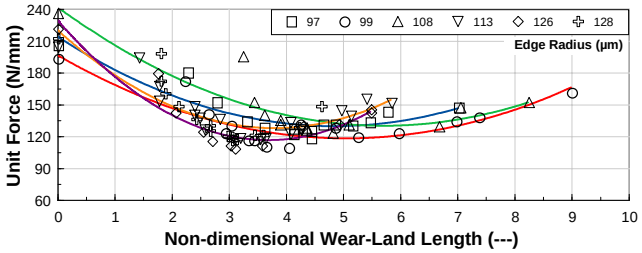

Figure 10 Blunt tool unit thrust force versus non-dimensional wear-land length

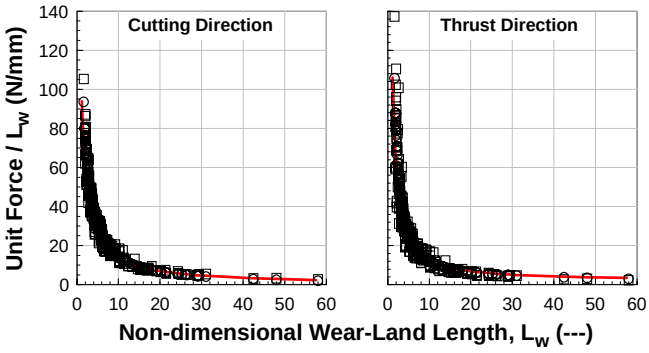

Figure 11 Blunt-tool unit force, per non-dimensional wear-land length, versus non-dimensional wear-land length

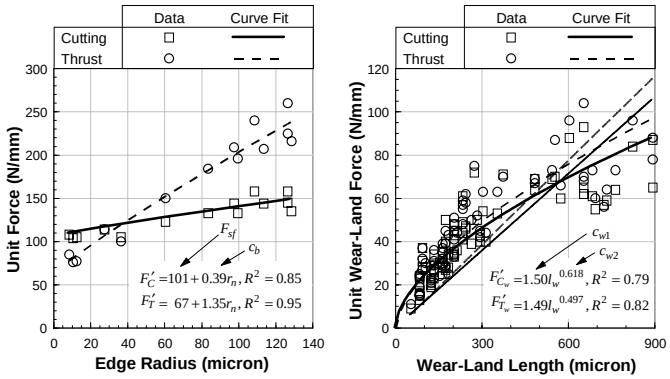

(a) (b)

Figure 12 Effect of edge radius and wear-land on unit forces: (a) fresh-tool edge radius effect, (b) parasitic wear-land force for no edge radius

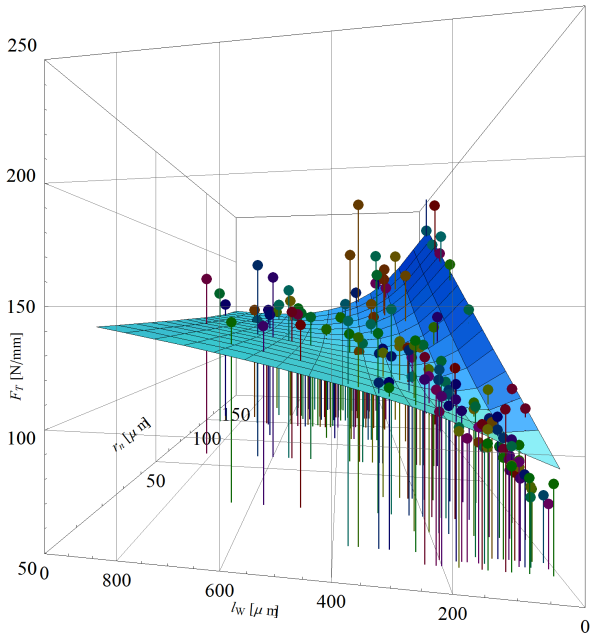

Figure 13 Nonlinear regression result (thrust) for the all-at-once fit to the proposed functional form

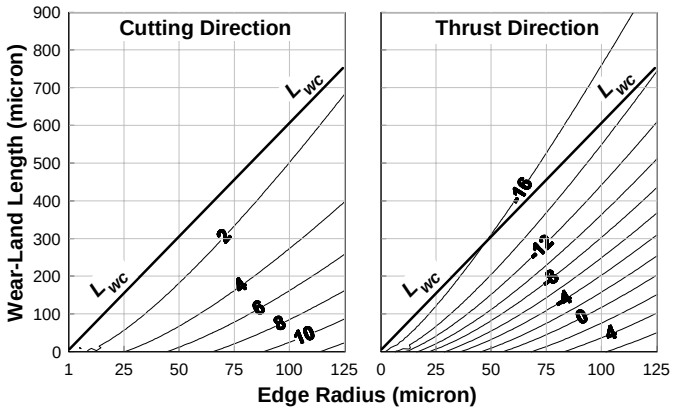

Figure 14 Percent deviation of piece-by-piece model relative to all-at-once model

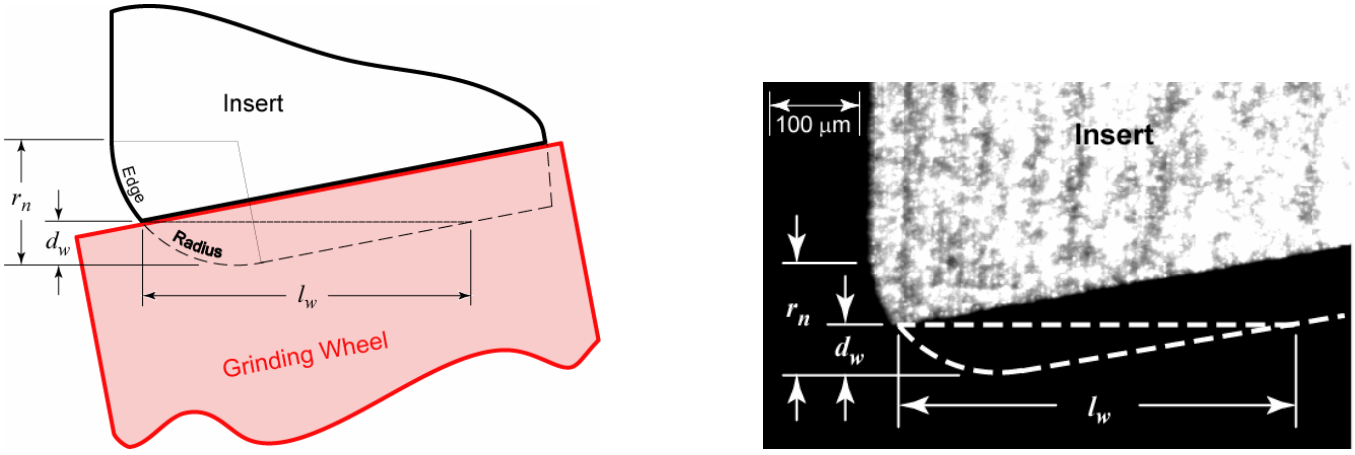

(a) (b)

Figure 15 Edge-sharpening to an equivalent wear-land l_w while not introducing the parasitic wear-land force: (a) sharpening procedure, (b) an actual edge.

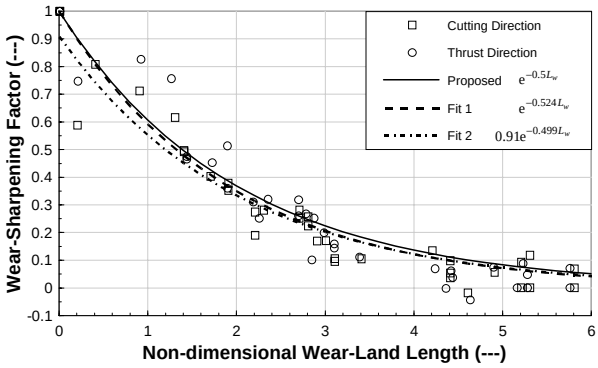

Figure 16 Wear-sharpening factor computed from edge-sharpening experiment showing proposed exponential model and a regression-fit exponential.